

Hadronic Processes in Advection-Dominated Accretion Flow as the Origin of TeV Excesses in BL Lac Objects

Ji-Shun Lian ¹, Ze-Rui Wang ², AND Jin Zhang† ¹

¹*School of Physics, Beijing Institute of Technology, Beijing 100081, People's Republic of China; j.zhang@bit.edu.cn*

²*College of Physics and Electronic Engineering, Qilu Normal University, Jinan 250200, People's Republic of China*

ABSTRACT

The spectral energy distributions (SEDs) of certain BL Lac objects (BL Lacs) exhibit an additional hard γ -ray component in the TeV energy range that surpasses the predictions of the one-zone leptonic jet model. The origin of this excess emission remains unclear. In this study, we selected five BL Lacs whose SEDs display a very hard intrinsic spectrum in the TeV band and successfully reproduced their broadband SEDs using a two-zone lepto-hadronic model. Within this framework, the emission observed in the optical, X-ray, GeV γ -ray, and sub-TeV γ -ray bands is modeled using the synchrotron and synchrotron self-Compton radiation processes of the relativistic electrons in the jets. Meanwhile, the TeV excess is attributed to γ -ray emission resulting from the photomeson ($p\gamma$) process via π^0 decay occurring within advection-dominated accretion flows (ADAFs). This scenario requires a hard proton spectrum with a spectral index of $p \sim 1.6 - 1.7$ and a cutoff energy ranging from 30 to 90 TeV, as well as a relatively large ADAF radius. Such hard proton spectra suggest that the dominant acceleration mechanisms are likely magnetic reconnection and/or stochastic acceleration processes within ADAFs. Additionally, the emission from the cascaded electrons results in a bump in the keV–MeV band; however, it is overwhelmed by the jet emission. Although the hadronuclear (pp) process cannot be entirely ruled out, it would necessitate an even harder proton spectrum and a higher cutoff energy compared to the $p\gamma$ process, making it a less favorable explanation for the observed TeV excess.

Keywords: gamma rays: galaxies – radiation mechanisms: non-thermal – accretion disks – galaxies: jets

1. INTRODUCTION

Blazars are a subclass of active galactic nuclei (AGNs) characterized by relativistic jets that are aligned closely with the observer's line of sight, typically within a few degrees ($< 5^\circ$, Ghisellini et al. 1993; Urry & Padovani 1995; Blandford et al. 2019). Blazars are further classified into flat spectrum radio quasars (FSRQs) and BL Lac objects (BL Lacs) on the basis of their optical spectral features; FSRQs exhibit prominent emission lines, while BL Lacs have weak or no emission lines (Stickel et al. 1991; Fan 2003; Giommi et al. 2012). According to the Fermi-LAT catalog data, BL Lacs generally demonstrate lower luminosity and harder spectra compared to FSRQs (Ajello et al. 2017). The jets of these two types of blazars are believed to differ in both composition and radiation efficiency (Ghisellini et al. 2014; Zhang et al. 2014), a distinction that is intrinsically linked to the varying accretion rates of their central supermassive black holes (SMBHs, Ghisellini et al. 2009; Giommi et al. 2013;

Ghisellini et al. 2014; Pei et al. 2022). Within the framework of unified models for radio-loud AGNs, BL Lacs and FSRQs are associated with Fanaroff-Riley type I (FR I) and type II (FR II) radio galaxies (Urry & Padovani 1995), respectively. These two types of radio galaxies are characterized by distinct accretion modes due to the different accretion rates (Mingo et al. 2014; Fernandes et al. 2015); the hot mode of a radiatively inefficient accretion flow (RIAF) for FR I radio galaxies and the cold mode of a standard thin accretion disk for FR II radio galaxies (Dermer & Giebels 2016; Rieger & Levinson 2018). Therefore, BL Lacs are likely to host a RIAF.

Blazars represent one of the primary extragalactic γ -ray emitting sources, especially in the TeV band, with the majority of detected TeV sources being BL Lacs¹. The broadband spectral energy distributions (SEDs) of BL Lacs typically exhibit a double-peaked structure, which is commonly attributed to synchrotron radiation and synchrotron self-Compton (SSC) processes of relativistic electrons (e.g., Maraschi et al. 1992; Ghisellini et al. 2010; Tavecchio et al.

Corresponding author: Jin Zhang
j.zhang@bit.edu.cn

¹ <http://tevcat2.uchicago.edu/> (Wakely & Horan 2008)

2010; Zhang et al. 2012; Yan et al. 2014). In general, this one-zone SSC model provides an adequate description of the BL Lac SEDs during quiescent states, such as those of BL Lacs Mrk 421 (Abdo et al. 2011) and H2356–309 (H. E. S. S. Collaboration et al. 2010). However, when sources exhibit high-flux activity in the X-ray and/or γ -ray bands or display a hard γ -ray spectrum in the TeV regime, more complex multi-zone models are often required to accurately reproduce the observed broadband emission (e.g., Błażejowski et al. 2005; Aharonian et al. 2007a). With a multiyear observational campaign conducted by the MAGIC Collaboration on 10 extreme high-frequency-peaked BL Lacs, Acciari et al. (2020) found that while the one-zone SSC model can still fit the data, it requires a critically low magnetization. In contrast, a spine-layer emission model offers a satisfactory solution to this magnetization problem. Furthermore, recent multi-wavelength photometric and polarization studies provide growing evidence in favor of multiple emission zones (e.g., Liodakis et al. 2022; MAGIC Collaboration et al. 2025). Additionally, the one-zone leptonic model encounters difficulties in accounting for the detection of a neutrino event associated with the BL Lac TXS 0506+056 (IceCube Collaboration et al. 2018). Therefore, hybrid leptonic–hadronic jet models have been proposed to explain such multi-messenger observations (Ansoldi et al. 2018; Keivani et al. 2018; Xue et al. 2019).

The radio-quiet Seyfert galaxy NGC 1068 has been confirmed as an astrophysical neutrino emitter (IceCube Collaboration et al. 2022), with the observed neutrinos likely originating from high-energy protons accelerated in the corona (e.g., Murase 2022; Das et al. 2024; Fiorillo et al. 2024; Mbarek et al. 2024). Similar mechanisms have also been proposed to explain the origin of γ -ray emission and to predict the potential neutrino flux from other Seyfert galaxies, including NGC 4151, NGC 4945, and Circinus galaxy (Murase et al. 2024), as well as the detected neutrino emission from the blazar TXS 0506+056 (Khattee Zathul et al. 2025; Yang et al. 2025). Moreover, Kimura et al. (2015) suggested that low-luminosity AGNs (LLAGNs) could generate high-energy neutrino emission via pp and/or $p\gamma$ interactions, where protons are accelerated stochastically by turbulent processes within RIAFs. These findings imply that disk-corona systems are likely also sources of γ -ray emission due to the presence of accelerated high-energy particles, where the disk-corona system includes RIAFs.

Some studies have suggested that the accretion mode of BL Lacs is the optically thin advection-dominated accretion flows (ADAFs, Wang et al. 2002; Chen et al. 2023; Zhao et al. 2024), which represents one of the most extensively studied RIAF models (Narayan & Yi 1994; Yuan 2007; Yuan & Narayan 2014). Within ADAFs, nonthermal protons can be accelerated by magnetic reconnections (Hoshino 2013;

Comisso & Sironi 2019a; Sun & Bai 2021), magnetohydrodynamic (MHD) turbulence (Becker et al. 2006; Stawarz & Petrosian 2008; Kimura et al. 2015, 2021b), or shocks (Stecker et al. 1991; Toma & Takahara 2012). In this paper, we investigate the radiation of high-energy protons within ADAFs to provide an explanation for the TeV γ -ray excess observed in five BL Lacs, a phenomenon defined in reference to the one-zone SSC model. The broadband SED data for the selected sources are presented in Section 2, while the details of the proposed model are outlined in Section 3. The model fitting strategies and corresponding results are given in Section 4. Discussion of fitting results and a summary are provided in Sections 5 and 6, respectively.

2. TEV-EXCESS SOURCES

This study includes five BL Lac SEDs that exhibit a significant TeV excess component, where the TeV excess is revealed based on the one-zone SSC model fitting results. Among these, four sources² are drawn from Cheng et al. (2022), with the TeV excess attributed to the $p\gamma$ process occurring within the jets. The selected SEDs of these five sources are illustrated in Figure 1, with the intrinsic TeV emission corrected based on the extragalactic background light (EBL) model provided by Finke et al. (2022). Additionally, based on the long-term light curves presented in the Fermi-LAT 14-year Source Catalog (4FGL-DR4)³, no significant variability is detected in the GeV band for these sources. Therefore, we also include the 14-year average spectra from the 4FGL-DR4 for these sources (with the exception of 1ES 0414+009) in Figure 1 to constrain the model parameters. Further details regarding the selected sources and their SEDs are outlined below.

- *1ES 0229+200*. A typical extreme high-synchrotron-peaked BL Lac at a redshift of $z = 0.1396$ (Woo et al. 2005), characterized by an extremely hard spectrum in both the X-ray and TeV γ -ray bands. Its TeV γ -ray emission was first detected by the High Energy Stereoscopic System (H.E.S.S.) telescopes in 2005 and 2006 (Aharonian et al. 2007b), with the spectrum extending up to 15 TeV and exhibiting a hard photon spectral index of $\Gamma_\gamma \sim 2.5$ (Aharonian et al. 2007b). As displayed in Figure 1, the TeV γ -ray data were obtained from observations with the H.E.S.S. telescopes in 2006 (Aharonian et al. 2007b), while the optical and X-ray data, collected in 2008, were provided by Swift-UVOT and Swift-XRT, respectively (Tavecchio et al. 2010).

² Mrk 421 is excluded due to its significant variability across multiple wavelengths, particularly in the TeV band.

³ https://fermi.gsfc.nasa.gov/ssc/data/access/lat/14yr_catalog/

- *H2356–309*. A high-synchrotron-peaked BL Lac located at a redshift of $z = 0.165$ (Falomo 1991). H2356–309 is a candidate neutrino emitter situated within the error circles of three IceCube events, suggesting that the TeV γ -ray emission could originate from hadronic processes (Sahu & Miranda 2015). The quasi-simultaneous broadband SED, as illustrated in Figure 1, is taken from H. E. S. S. Collaboration et al. (2010). It includes optical/UV and X-ray observations conducted by XMM-Newton on 15 June 2005, as well as the time-averaged very high energy (VHE) γ -ray spectra obtained from observations with the H.E.S.S. telescopes in 2005.
- *1ES 1101–232*. A high-synchrotron-peaked BL Lac located at a redshift of $z = 0.186$ (Falomo et al. 1994). Its VHE γ -ray emission was first detected by the H.E.S.S. telescopes during observations conducted in 2004 and 2005 (Aharonian et al. 2007a). The source displayed an exceptionally hard spectrum, with a photon spectral index of $\Gamma_\gamma \sim 1.5$ in the energy range of 0.23–4 TeV, and no significant variability in the VHE γ -ray flux was observed across any time scale. The quasi-simultaneous SED, as illustrated in Figure 1, incorporates X-ray and optical data obtained from XMM-Newton observations on 8 June 2004, as well as H.E.S.S. data collected between 5 and 16 March 2005.
- *1ES 0347–121*. An extremely high-synchrotron-peaked BL Lac located at a redshift of $z = 0.188$ (Woo et al. 2005). The VHE γ -ray emission from this source was first detected by the H.E.S.S. telescopes in 2006 (Aharonian et al. 2007c). The possibility of a hadronic jet origin for its VHE emission has been investigated in Cerruti et al. (2015). The H.E.S.S. observational data, together with the simultaneous X-ray and UV/optical data obtained from Swift and the Automatic Telescope for Optical Monitoring, are retrieved from Aharonian et al. (2007c) and used to construct the broadband SED, as shown in Figure 1.
- *1ES 0414+009*. One of the most distant TeV BL Lacs detected to date, located at a redshift of $z = 0.287$ (Halpern et al. 1991). Its VHE γ -ray emission was first detected by the H.E.S.S. telescopes during observations conducted between October 2005 and December 2009 (H. E. S. S. Collaboration et al. 2012). The source was also detected by VERITAS between January 2008 and February 2011 (Aliu et al. 2012). Broadband data, including optical observations from the Michigan-Dartmouth-MIT Observatory, X-ray data from Swift, GeV observations from Fermi-LAT, and the VERITAS spectrum, indicate that a homogeneous one-zone leptonic model is insufficient to accurately describe the

broadband SED of 1ES 0414+009. In contrast, a leptohadronic model provides a better fit to the data (Aliu et al. 2012). The selected broadband SED of 1ES 0414+009, as shown in Figure 1, is obtained from H. E. S. S. Collaboration et al. (2012).

3. MODEL

The one-zone leptonic jet model is commonly used to fit the observed broadband SEDs of TeV-emitting BL Lacs (e.g., Tavecchio et al. 2010; Zhang et al. 2012). In this work, a two-zone lepto-hadronic model is employed to account for the broadband SEDs of the five BL Lacs. The observed optical, X-ray, and GeV γ -ray emission is attributed to the synchrotron and SSC processes of the relativistic electrons within the jets, following a similar approach to that in Tavecchio et al. (2010) and Zhang et al. (2012). Meanwhile, the TeV excess emission, which exceeds the predictions of the one-zone SSC model, is interpreted as the decay of neutral pions produced via $p\gamma$ interactions within the ADAFs.

3.1. Leptonic Radiation within the Jet

The emission region is modeled as a sphere with a radius of R_b and magnetic field strength of B_{jet} , as adopted in previous studies (e.g., Zhang et al. 2012; Chen 2017; Xue & Wang 2021; Wang et al. 2022). The size of the emission region is derived with the variability timescale (Δt) using the relation $R_b = c\Delta t\delta_D/(1+z)$, where δ_D denotes the Doppler factor, and c is the speed of light. We assume $\delta_D = \Gamma$ for these BL Lacs, where Γ is the bulk Lorentz factor of the emission region. The energy distribution of relativistic electrons is described by a broken power-law function, defined by a normalization constant $N_{e,0}$, a break energy $\gamma_{e,b}$, and power-law indices p_1 and p_2 below and above the break energy, respectively, within the energy range $[\gamma_{e,\text{min}}, \gamma_{e,\text{max}}]$. The synchrotron and SSC processes of relativistic electrons, along with the effects of synchrotron self-absorption and Klein-Nishina, are incorporated into the leptonic model calculations.

3.2. Lepto-hadronic Radiation within the ADAF

BL Lacs are believed to harbor an ADAF in the central region near the SMBHs. ADAF is characterized by being geometrically thick, optically thin, and having low radiative efficiency (e.g., Rees et al. 1982; Ichimaru 1977; Narayan & Yi 1994; Yuan 2007; Yuan & Narayan 2014). Within ADAFs, thermal electrons and ions lose energy through synchrotron emission, bremsstrahlung, and inverse Comptonization of seed photons generated by these two radiative processes, thereby producing the ADAF emission spectrum across the electromagnetic spectrum from radio to hard X-ray bands. Using the parameter values listed in Table 1, we numerically compute the global structure and dynamics of the flows following the methods outlined in Yuan et al. (2000, 2003) to

calculate the ADAF spectrum. For further details, please refer to Yuan et al. (2005, 2007) and Nemmen et al. (2014). The parameters include the SMBH mass (M_{BH}), the power-law index of radial variation (s), the viscosity parameter (α), the ratio of gas pressure to total pressure (β), the adiabatic index (γ_{adi}), the outer radius of the ADAF (R_0), the fraction of the turbulent energy that heats the electrons (δ_{ADAF}), and the accretion rate (\dot{m}).

We hypothesize the existence of relativistic protons accelerated within the ADAFs of these BL Lacs. The energy distribution of these protons is assumed to follow an exponential cutoff power-law function, characterized by a spectral index p and a cutoff energy $\varepsilon_{p,\text{cut}}$, within the energy range $[\varepsilon_{p,\text{min}}, \varepsilon_{p,\text{max}}]$, i.e.,

$$N_p(\varepsilon_p) = N_{p,0} \left(\frac{\varepsilon_p}{1\text{eV}} \right)^{-p} \exp\left(-\frac{\varepsilon_p}{\varepsilon_{p,\text{cut}}}\right). \quad (1)$$

These protons interact with photons emitted by the ADAF through the $p\gamma$ process. Both photomeson production and the Bethe–Heitler process ($p\gamma \rightarrow p + e^+ + e^-$) are taken into account. It is assumed that the relevant hadronic processes occur within a spherical ADAF of radius R_0 . The viscosity parameter of the ADAFs is set to $\alpha \sim 0.3$; therefore, the accretion flow is quasi-spherical rather than toroidal (Narayan et al. 1998).

The photomeson process is calculated using a semi-analytical method. The proton energy loss rate is given by

$$t_{p\gamma}^{-1}(\varepsilon_p) = \frac{c}{2\gamma_p^2} \int_{\bar{\varepsilon}_{\text{th}}}^{\infty} d\bar{\varepsilon} \sigma_{p\gamma}(\bar{\varepsilon}) \kappa_{p\gamma}(\bar{\varepsilon}) \bar{\varepsilon} \int_{\bar{\varepsilon}/2\gamma_p}^{\infty} d\varepsilon \varepsilon^{-2} n_\varepsilon, \quad (2)$$

where ε_p and ε are the proton and photon energies in the ADAF frame, respectively; $\bar{\varepsilon}$ is the photon energy in the proton frame; $\sigma_{p\gamma}$ and $\kappa_{p\gamma}$ are the photomeson cross section and the proton inelasticity, respectively (for details, see Stecker 1968; Chodorowski et al. 1992; Atayan & Dermer 2003; Romero & Vila 2008; Cheng et al. 2022). Relativistic protons lose energy through pion production, which includes single-pion and multi-pion branching processes as described by

$$p + \gamma \rightarrow \begin{cases} p + a\pi^0 + b(\pi^+ + \pi^-), \\ n + \pi^+ + a\pi^0 + b(\pi^+ + \pi^-), \end{cases} \quad (3)$$

where a and b are the pion multiplicities (Romero & Vila 2008). Subsequently, the produced pions decay further as follows:

$$\begin{aligned} \pi^+ &\rightarrow \mu^+ + \nu_\mu, & \mu^+ &\rightarrow e^+ + \nu_e + \bar{\nu}_\mu, \\ \pi^- &\rightarrow \mu^- + \bar{\nu}_\mu, & \mu^- &\rightarrow e^- + \bar{\nu}_e + \nu_\mu, \\ \pi^0 &\rightarrow \gamma\gamma. \end{aligned} \quad (4)$$

The observed TeV excess in the broadband SEDs of the five BL Lacs is attributed to the decay of π^0 mesons.

The potential influence of hadron-triggered electromagnetic cascade processes within the ADAF is also investigated. The cascade processes involve electrons that are injected through $\gamma\gamma$ annihilation, the photopion process, and the Bethe–Heitler process. The Bethe–Heitler process is computed using a semi-analytical method in the framework established by Kelner & Aharonian (2008). The distribution of cascaded electrons is determined through a time-independent approach by iteratively solving the isotropic Fokker-Planck equation under equilibrium conditions (Böttcher et al. 2013):

$$\frac{\partial}{\partial \gamma_e} (\dot{\gamma}_e N_e^{\text{cas}}) = Q_e(\gamma_e) + \dot{N}_e^{\gamma\gamma}(\gamma_e) + \dot{N}_e^{\text{esc}}(\gamma_e), \quad (5)$$

where Q_e represents the total electron injection resulting from the Bethe–Heitler and photomeson processes, $\dot{N}_e^{\gamma\gamma}$ denotes the electron injection from internal $\gamma\gamma$ interactions, \dot{N}_e^{esc} accounts for the escape term, and N_e^{cas} indicates the cascade electron distribution. The cascaded electrons lose energy primarily through synchrotron and SSC processes.

4. FITTING STRATEGIES AND RESULTS

The broadband SEDs of the five BL Lacs are modeled using the synchrotron and SSC emission processes from a single population of relativistic electrons within the jets, as well as the radiation triggered by a single population of protons accelerated in ADAFs.

Firstly, we use the leptonic jet radiation to account for the observed SEDs, while ignoring the TeV flux fitting. The leptonic jet model incorporates the following parameters: B_{jet} , Δt , δ_{D} , p_1 , p_2 , $\gamma_{e,\text{min}}$, $\gamma_{e,\text{b}}$, $\gamma_{e,\text{max}}$, and $N_{e,0}$. Except for 1ES 0414+009, the same set of observational data was adopted for the remaining sources studied in Cheng et al. (2022), where the same leptonic model was applied to reproduce the broadband SEDs of the five BL Lacs. Consequently, comparable values for the fitting parameters are obtained in this study. For 1ES 0414+009, the variability timescale is from Aliu et al. (2012). The derived parameter values are expected to be broadly consistent with those reported in previous studies of these five BL Lacs, where the one-zone synchrotron+SSC model was similarly applied to interpret the broadband SEDs (e.g., Aharonian et al. 2007c; Costamante 2007; H. E. S. S. Collaboration et al. 2010; Tavecchio et al. 2010; Zhang et al. 2012). A summary of all fitted parameters is provided in Table 1, and the corresponding fitting results are illustrated in Figure 1.

Secondly, the ADAF emission spectrum resulting from thermal electrons and ions is calculated based on the following parameters: M_{BH} , s , α , β , γ_{adi} , R_0 , δ_{ADAF} , and \dot{m} . During the calculations, we fix the values of $s = 0.3$, $\alpha = 0.3$, $\beta = 0.9$, $\gamma_{\text{adi}} = 1.5$, and $R_0 = 10^4 R_S$ (R_S is the Schwarzschild radius) for all sources. The values of M_{BH} for each source are listed in Table 1, along with the corresponding references.

The accretion rate is defined as $\dot{m} = \dot{M}/\dot{M}_{\text{Edd}}$, where \dot{M} represents the SMBH accretion rate, and $\dot{M}_{\text{Edd}} = L_{\text{Edd}}/\eta c^2$ denotes the Eddington accretion rate. Here, L_{Edd} refers to the Eddington luminosity, $\eta = \frac{L_{\text{disk}}}{\dot{M}c^2}$ (Frank et al. 1992; Narayan et al. 1998) is the radiative efficiency, and L_{disk} corresponds to the disk luminosity. Therefore, the accretion rate can also be expressed as $\dot{m} = \frac{L_{\text{disk}}}{L_{\text{Edd}}}$. Since the directly measured L_{disk} values for these five BL Lacs are unavailable, the luminosity at 10^{15} Hz from the leptonic jet model fitting curve is used as an approximation for L_{disk} to compute the corresponding accretion rates⁴, as summarized in Table 1. At this stage, only δ_{ADAF} remains as a free parameter. Once δ_{ADAF} is fixed, the ADAF spectrum of thermal electron and ion emission can be derived. The parameter δ_{ADAF} is generally assumed to lie within the range of 0.1 to 0.5 (Yuan & Narayan 2014). We primarily set it to 0.5, although minor adjustments may be made to optimize the ADAF photon fields for the $p\gamma$ process.

Subsequently, the spectrum of the relativistic proton radiations through the photomeson and cascade processes is modeled using the parameters: R_0 , the magnetic field strength (B_{ADAF}) within the ADAF, and the proton distribution parameters (p , $\varepsilon_{p,\text{min}}$, $\varepsilon_{p,\text{cut}}$, $\varepsilon_{p,\text{max}}$, $N_{p,0}$). It should be noted that the target photons involved in the $p\gamma$ process are considered exclusively from the ADAF spectrum. The values of R_0 have been fixed as previously described. The magnetic field strength within ADAFs, from the inner to the outer regions, is determined by the following relation (Yuan & Narayan 2014)

$$B_{\text{ADAF}} \approx 6.5 \times 10^8 (1 + \beta)^{-1/2} \alpha^{-1/2} M_{\text{BH}}^{-1/2} \dot{m}^{1/2} r^{-5/4+s/2} \text{ G}, \quad (6)$$

where $r \equiv R/R_S$, and R is the radius within $R_S \leq R \leq R_0$. Based on this equation, we assume a uniform magnetic field with an average value of $B_{\text{ADAF}} = 1$ G, which is also consistent with results given in other studies (e.g., Yuan et al. 2003; Kimura et al. 2015, 2019, 2021b). Accordingly, $B_{\text{ADAF}} = 1$ G is applied to the five BL Lacs.

Finally, based on the results of the leptonic jet fitting, the proton distribution parameters and the value of δ_{ADAF} are adjusted to model the TeV excess component in the SEDs of five BL Lacs. Our numerical results are presented in Figure 1, and the corresponding model parameters are summarized in Table 1. It is evident that the model well reproduces the observational data. However, it should be noted that the quality of the SED fits is assessed visually. The model param-

⁴ In this case, the accretion rates of the sources may be overestimated, leading to an overestimation of the luminosity of ADAFs. This, in turn, results in a lower proton number density or a softer proton spectral index when modeling the observational data. However, this effect is negligible. A decrease in ADAF luminosity by one order of magnitude would require only a minor adjustment of approximately 0.1 in the proton spectral index.

eters cannot be rigorously constrained, and we therefore only identify a parameter set that can represent the SEDs.

As presented in Table 1, a hard proton spectrum with an index of $p \sim 1.6 - 1.7$, along with cutoff energies ranging from 30 TeV to 90 TeV, is required to account for the TeV excess observed in the SEDs of the five BL Lacs. As illustrated in Figure 1, this TeV excess is attributed to the decay of π^0 mesons produced through $p\gamma$ interactions within the ADAFs. The ADAF emission spectra (magenta solid lines) from thermal particles, as well as the synchrotron emission (red dashed lines) originating from cascaded electrons, are significantly overwhelmed by the leptonic jet emission. Additionally, we estimate the proton number density (N_p) in the energy range [$E_{p,\text{cut}} \times 10^{-3}, E_{p,\text{cut}} \times 10$] and obtain $N_p \sim 10^{4-7} \text{ cm}^{-3}$, as listed in Table 1. These values do not exceed the typical proton number densities of ADAFs, which range from approximately 10^4 to 10^{10} cm^{-3} from the outer to the inner regions (e.g., Yuan & Narayan 2014; Kimura et al. 2015, 2021a,b; Bougheliiba et al. 2022).

5. DISCUSSION

5.1. Proton Acceleration within ADAF

The main challenge for the model is to determine whether protons can be accelerated to such high energies within ADAFs. The maximum attainable energy of charged particles is determined by the Hillas criterion (Hillas 1984), which requires that the size of the acceleration region exceeds the Larmor radius of the particles. According to this criterion, the maximum proton energy can be given by

$$E_{\text{max}} = 10^{21} \text{ eV} \left(\frac{R_L}{1 \text{ pc}} \right) \left(\frac{B}{1 \text{ G}} \right) \left(\frac{u}{c} \right), \quad (7)$$

where the Larmor radius is assumed to be $R_L = R_0 = 10^4 R_S$, and the magnetic field strength is taken as $B = B_{\text{ADAF}} = 1$ G. In the context of diffusive shock acceleration, u denotes the shock velocity with a typical value of $\sim 0.1c$ (Rieger et al. 2007); in magnetic reconnection scenarios, u refers to some flow velocity comparable to the Alfvén speed, which is similarly $\sim 0.1c$ (Matthews et al. 2020). Therefore, protons can potentially be accelerated to energies of up to $E_{\text{max}} \sim 10^{20}$ eV within ADAFs.

In RIAFs, the plasma becomes collisionless under conditions of low accretion rates, thereby enabling the presence of non-thermal particles (Narayan & Yi 1994; Mahadevan 1997; Toma & Takahara 2012). In early hadronic models of AGNs, accretion shocks were proposed as potential sites for particle acceleration (e.g., Stecker et al. 1991). However, numerical simulations have not yet confirmed the existence of such shocks (Kimura et al. 2019). Shocks may arise from the collision of fallback material (Alvarez-Muñiz & Mészáros 2004) or from failed winds originating from the accretion disk. In such scenarios, a spectral index of $p \sim 2$ is

expected and has been assumed (Alvarez-Muñiz & Mészáros 2004; Inoue et al. 2020). Additionally, the magnetorotational instability (MRI) within RIAFs has long been considered as a mechanism for generating effective viscosity and strong magnetic turbulence, which are essential for angular momentum transport (e.g., Balbus & Hawley 1991; Sano et al. 2004). MRI-driven magnetic reconnection can accelerate protons to energies exceeding the PeV range, with spectra as hard as $p < 2$, particularly under conditions of high magnetization and enhanced turbulence near SMBHs (e.g., Hoshino 2013; Comisso & Sironi 2019b; Sun & Bai 2021). Alternatively, MRI can generate strong MHD turbulence that scatters protons within RIAFs. This stochastic acceleration mechanism is expected to yield a hard proton spectrum with $p < 1$, with a cutoff occurring around 10–100 PeV due to photo-hadronic interactions (e.g., Becker et al. 2006; Stawarz & Petrosian 2008; Kimura et al. 2015, 2021b). In the case of BL Lacs, the jet is launched from the polar region of the SMBHs, and high-energy protons may also be accelerated via shear acceleration at the jet base (Sun & Bai 2021; Murase 2022).

Previous studies have commonly assumed a power-law proton distribution with a spectral index of $p \sim 2 - 4$, which is theoretically expected when protons are accelerated via the first-order Fermi mechanism (e.g., Inoue et al. 2019; Xue et al. 2021; Cheng et al. 2022; Xue et al. 2023). In our model, protons must be accelerated to energies ranging from 30 TeV to 90 TeV, with a relatively hard spectral index of $p \sim 1.6 - 1.7$. This suggests that magnetic reconnection and/or stochastic acceleration may be the dominant acceleration mechanisms for protons in ADAFs. Based on the stochastic particle acceleration mechanism and a power-law spectrum with $p < 5/3$, Kimura et al. (2015) demonstrated that nonthermal protons accelerated within the RIAFs of low-luminosity AGNs can generate detectable GeV γ -rays and neutrons through pp and/or $p\gamma$ interactions.

5.2. Contributions of the pp Process

The high-energy protons can also produce TeV photons via the pp process. Therefore, we calculate the pp process using the method developed by Kafexhiu et al. (2014), which provides analytical parametrizations for the energy spectra and production rates of γ -rays resulting from pp interactions. Firstly, we adopt the same proton spectrum and spectral parameter values as those used in the $p\gamma$ process, under the assumption that sufficient cold target protons are present, to calculate the possible γ -ray spectrum for these BL Lacs. As shown in Figure 1, the γ -ray spectrum (represented by gray dashed lines) generated by the pp process is insufficiently hard in the TeV energy range to adequately fit the observed data. If the TeV excess is assumed to be predominantly attributed to the pp process, a significantly harder proton spectrum with a higher cutoff energy (exceeding 1 PeV) would

be required to accurately reproduce the observational data, compared to the $p\gamma$ process. This scenario imposes more stringent requirements on the underlying particle acceleration mechanism. Therefore, we propose that the $p\gamma$ process is more favorable than the pp process for explaining the TeV excess observed in these BL Lacs.

5.3. $\gamma\gamma$ Absorption and Cascaded Electron Emission in ADAF

High-energy γ -ray photons originating from π^0 decay interact with low-energy target photons from the ADAF through the two-photon annihilation process, $\gamma\gamma \rightarrow e^+e^-$. The typical energy of a target photon involved in such an interaction with a TeV photon is given by $\epsilon_t = m_e^2 c^4 / \epsilon_\gamma \simeq 0.26 (1 \text{ TeV} / \epsilon_\gamma) \text{ eV}$. Using the source 1ES 0347–121 as a case study, we compute the optical depth curves as a function of γ -ray photon energy for various ADAF sizes, as shown in Figure 2. The results indicate that TeV photons are unable to escape the ADAF due to significant $\gamma\gamma$ absorption when the ADAF radius is too small. A minimum radius of $R_0 > 1000R_s$ is required to account for the observed TeV excess. Similar findings have been reported in earlier studies (e.g. Eichmann et al. 2022; Murase 2022; Ajello et al. 2023). Recently, Liu et al. (2025) suggested that the extended corona ($> 10^6$ gravitational radii) in radio-quiet Seyfert galaxies can produce γ -rays with energies exceeding several GeV.

The cascaded electrons generated by the $\gamma\gamma$ annihilation process, along with those produced via the $p\gamma$ interaction, can trigger electromagnetic emission, leading to a keV–MeV emission component in the SEDs (e.g., Cheng et al. 2022; Murase 2022). However, due to the weak $\gamma\gamma$ absorption under an ADAF radius of $10^4 R_s$, the emission from cascaded electrons is found to be insignificant compared to jet radiation in the five BL Lacs, as shown in Figure 1. Therefore, BL Lacs with smaller ADAF radii may serve as promising candidates for testing our model, as these sources do not exhibit a significant TeV excess, yet display a distinct keV–MeV excess in their SEDs.

5.4. Implications for Variability and Neutrino Detection

To avoid the $\gamma\gamma$ absorption effect, a large ADAF radius is required in the model to reproduce the observed TeV excess, i.e., $R_0 \sim 10^4 R_s$, with a minimum of $R_0 \sim 10^3 R_s$. Within the framework of this model, the derived minimum variability time-scale of TeV emission ranges from several months to years. Therefore, the model is unable to account for the TeV spectra observed during short-term flaring episodes. Among the five SEDs selected in our sample, only the VHE flux from H 2356–309 exhibited low-amplitude variations on timescales of months to years during its TeV detections; however, no significant variability on shorter timescales was observed (H. E. S. S. Collaboration et al. 2010). For all other

sources, no notable variation in the TeV flux was observed across any timescale (Aharonian et al. 2007a,b,c; H. E. S. S. Collaboration et al. 2012). This constitutes the primary rationale for excluding Mrk 421 from our sample: although its SED exhibits a TeV excess component during high-flux states and it is included in the study by Cheng et al. (2022), its highly variable TeV emission is inconsistent with the assumed emission scenario of the model.

As shown in Formula 4, the model predicts neutrino radiation. Within this theoretical framework, we compute the neutrino flux produced via the $p\gamma$ process and present the results for each source in Figure 1. The total neutrino flux corresponds to the sum of the muon neutrino and muon antineutrino components. The differential sensitivity curves of IceCube for three different declinations, which are obtained from Aartsen et al. (2019), are also present in Figure 1. It is evident that, with the exception of 1ES 0229+200, where the predicted neutrino flux slightly overlaps with IceCube’s sensitivity curves, the model-predicted fluxes for the remaining four sources fall significantly below IceCube’s detection thresholds. We further calculate the neutrino event rate using the formula from Aartsen et al. (2020):

$$\frac{dN_{\nu+\bar{\nu}}}{dt} = \int_0^\infty A_{\text{eff}}^{\nu+\bar{\nu}}(E_\nu, \delta_{\text{decl}}) \times \phi_{\nu+\bar{\nu}}(E_\nu) dE_\nu, \quad (8)$$

where A_{eff} denotes the IceCube point-like source effective area for muon neutrinos and muon antineutrinos at declination δ_{decl} , and E_ν and $\phi_{\nu+\bar{\nu}}(E_\nu)$ represent the neutrino energy and the differential neutrino energy flux, respectively. The estimated astrophysical neutrino event rates are 2.2 yr^{-1} for 1ES 0229+200, 0 yr^{-1} for H2356–309, $2.4 \times 10^{-2} \text{ yr}^{-1}$ for 1ES 1101–232, $1.6 \times 10^{-2} \text{ yr}^{-1}$ for 1ES 0347–121, and $4.7 \times 10^{-1} \text{ yr}^{-1}$ for 1ES 0414+009.

6. SUMMARY

In this work, we explored the potential hadronic origin of the observed TeV excess—defined within the framework of the one-zone SSC model—in the SEDs of five BL Lacs (1ES 0229+200, H2356–309, 1ES 1101–232, 1ES 0347–121, and 1ES 0414+009) using a two-zone lepto-hadronic model. The synchrotron radiation and SSC processes of relativistic electrons within jets account for the emission across the radio, optical, X-ray, and GeV γ -ray bands. The TeV γ -ray emission, which exceeds the predictions of the leptonic jet model, is attributed to proton-related emission within ADAFs. Although the $p\gamma$ process is primarily considered, the contribution from pp interactions cannot be entirely ruled out. The model successfully reproduces the broadband SEDs of the five BL Lacs by invoking a population of protons with a hard spectral index of approximately 1.6–1.7 and a cut-off energy in the range of 30–90 TeV within the ADAFs. We propose that these protons are accelerated via magnetic reconnection and/or stochastic acceleration mechanisms within

the ADAFs. We also considered the contribution from cascaded electrons generated by hadronic processes; however, this component is significantly overshadowed by the dominant jet emission. Furthermore, for the TeV photons to escape the emission region without being absorbed via $\gamma\gamma$ annihilation process, a large ADAF radius is required, resulting in a weak cascaded emission component in the keV–MeV band. Based on the fitting results and theoretical calculations, we suggest that BL Lacs with smaller ADAF radii may exhibit a prominent keV–MeV spectral bump without a corresponding TeV excess, making them ideal candidates for testing our model. Additionally, the requirement of a large ADAF radius implies that the model cannot readily account for the TeV emission observed during short-timescale flaring events.

ACKNOWLEDGMENTS

We thank the anonymous referee for the valuable suggestions and comments. We are grateful to Liang Chen and Da-Bin Lin for the valuable discussion. This work is supported by the National Key R&D Program of China (grant 2023YFE0117200) and the National Natural Science Foundation of China (grants 12203024, 12022305, 11973050, 12473042, and 12373109).

REFERENCES

- Aartsen, M. G., Ackermann, M., Adams, J., et al. 2019, *European Physical Journal C*, 79, 234, doi: [10.1140/epjc/s10052-019-6680-0](https://doi.org/10.1140/epjc/s10052-019-6680-0)
- . 2020, *PhRvL*, 124, 051103, doi: [10.1103/PhysRevLett.124.051103](https://doi.org/10.1103/PhysRevLett.124.051103)
- Abdo, A. A., Ackermann, M., Ajello, M., et al. 2011, *ApJ*, 736, 131, doi: [10.1088/0004-637X/736/2/131](https://doi.org/10.1088/0004-637X/736/2/131)
- Acciari, V. A., Ansoldi, S., Antonelli, L. A., et al. 2020, *ApJS*, 247, 16, doi: [10.3847/1538-4365/ab5b98](https://doi.org/10.3847/1538-4365/ab5b98)
- Aharonian, F., Akhperjanian, A. G., Bazer-Bachi, A. R., et al. 2007a, *A&A*, 470, 475, doi: [10.1051/0004-6361:20077057](https://doi.org/10.1051/0004-6361:20077057)
- Aharonian, F., Akhperjanian, A. G., Barres de Almeida, U., et al. 2007b, *A&A*, 475, L9, doi: [10.1051/0004-6361:20078462](https://doi.org/10.1051/0004-6361:20078462)
- . 2007c, *A&A*, 473, L25, doi: [10.1051/0004-6361:20078412](https://doi.org/10.1051/0004-6361:20078412)
- Ajello, M., Murase, K., & McDaniel, A. 2023, *ApJL*, 954, L49, doi: [10.3847/2041-8213/acf296](https://doi.org/10.3847/2041-8213/acf296)
- Ajello, M., Atwood, W. B., Baldini, L., et al. 2017, *ApJS*, 232, 18, doi: [10.3847/1538-4365/aa8221](https://doi.org/10.3847/1538-4365/aa8221)
- Aliu, E., Archambault, S., Arlen, T., et al. 2012, *ApJ*, 755, 118, doi: [10.1088/0004-637X/755/2/118](https://doi.org/10.1088/0004-637X/755/2/118)
- Alvarez-Muñiz, J., & Mészáros, P. 2004, *PhRvD*, 70, 123001, doi: [10.1103/PhysRevD.70.123001](https://doi.org/10.1103/PhysRevD.70.123001)
- Ansoldi, S., Antonelli, L. A., Arcaro, C., et al. 2018, *ApJL*, 863, L10, doi: [10.3847/2041-8213/aad083](https://doi.org/10.3847/2041-8213/aad083)
- Atoyan, A. M., & Dermer, C. D. 2003, *ApJ*, 586, 79, doi: [10.1086/346261](https://doi.org/10.1086/346261)
- Balbus, S. A., & Hawley, J. F. 1991, *ApJ*, 376, 214, doi: [10.1086/170270](https://doi.org/10.1086/170270)
- Becker, P. A., Le, T., & Dermer, C. D. 2006, *ApJ*, 647, 539, doi: [10.1086/505319](https://doi.org/10.1086/505319)
- Blandford, R., Meier, D., & Readhead, A. 2019, *ARA&A*, 57, 467, doi: [10.1146/annurev-astro-081817-051948](https://doi.org/10.1146/annurev-astro-081817-051948)
- Błażejowski, M., Blaylock, G., Bond, I. H., et al. 2005, *ApJ*, 630, 130, doi: [10.1086/431925](https://doi.org/10.1086/431925)
- Böttcher, M., Reimer, A., Sweeney, K., & Prakash, A. 2013, *ApJ*, 768, 54, doi: [10.1088/0004-637X/768/1/54](https://doi.org/10.1088/0004-637X/768/1/54)
- Boughelilba, M., Reimer, A., & Merten, L. 2022, *ApJ*, 938, 79, doi: [10.3847/1538-4357/ac8e64](https://doi.org/10.3847/1538-4357/ac8e64)
- Cerruti, M., Zech, A., Boisson, C., & Inoue, S. 2015, *MNRAS*, 448, 910, doi: [10.1093/mnras/stu2691](https://doi.org/10.1093/mnras/stu2691)
- Chen, L. 2017, *ApJ*, 842, 129, doi: [10.3847/1538-4357/aa7744](https://doi.org/10.3847/1538-4357/aa7744)
- Chen, Y., Gu, Q., Fan, J., et al. 2023, *MNRAS*, 526, 4079, doi: [10.1093/mnras/stad2623](https://doi.org/10.1093/mnras/stad2623)
- Cheng, J.-G., Huang, X.-L., Wang, Z.-R., Huang, J.-K., & Liang, E.-W. 2022, *ApJL*, 925, L19, doi: [10.3847/2041-8213/ac4d8e](https://doi.org/10.3847/2041-8213/ac4d8e)
- Chodorowski, M. J., Zdziarski, A. A., & Sikora, M. 1992, *ApJ*, 400, 181, doi: [10.1086/171984](https://doi.org/10.1086/171984)
- Comisso, L., & Sironi, L. 2019a, *ApJ*, 886, 122, doi: [10.3847/1538-4357/ab4c33](https://doi.org/10.3847/1538-4357/ab4c33)
- Comisso, L., & Sironi, L. 2019b, in *APS Meeting Abstracts*, Vol. 2019, APS Division of Plasma Physics Meeting Abstracts, TM9.002
- Costamante, L. 2007, *Ap&SS*, 309, 487, doi: [10.1007/s10509-007-9418-7](https://doi.org/10.1007/s10509-007-9418-7)
- Das, A., Zhang, B. T., & Murase, K. 2024, *ApJ*, 972, 44, doi: [10.3847/1538-4357/ad5a04](https://doi.org/10.3847/1538-4357/ad5a04)
- Dermer, C. D., & Giebels, B. 2016, *Comptes Rendus Physique*, 17, 594, doi: [10.1016/j.crhy.2016.04.004](https://doi.org/10.1016/j.crhy.2016.04.004)
- Eichmann, B., Oikonomou, F., Salvatore, S., Dettmar, R.-J., & Tjus, J. B. 2022, *ApJ*, 939, 43, doi: [10.3847/1538-4357/ac9588](https://doi.org/10.3847/1538-4357/ac9588)
- Falomo, R. 1991, *AJ*, 101, 821, doi: [10.1086/115726](https://doi.org/10.1086/115726)
- Falomo, R., Carangelo, N., & Treves, A. 2003, *MNRAS*, 343, 505, doi: [10.1046/j.1365-8711.2003.06690.x](https://doi.org/10.1046/j.1365-8711.2003.06690.x)
- Falomo, R., Scarpa, R., & Bersanelli, M. 1994, *ApJS*, 93, 125, doi: [10.1086/192048](https://doi.org/10.1086/192048)
- Fan, J. H. 2003, *ApJL*, 585, L23, doi: [10.1086/374033](https://doi.org/10.1086/374033)
- Fernandes, C. A. C., Jarvis, M. J., Martínez-Sansigre, A., et al. 2015, *MNRAS*, 447, 1184, doi: [10.1093/mnras/stu2517](https://doi.org/10.1093/mnras/stu2517)
- Finke, J. D., Ajello, M., Domínguez, A., et al. 2022, *ApJ*, 941, 33, doi: [10.3847/1538-4357/ac9843](https://doi.org/10.3847/1538-4357/ac9843)
- Fiorillo, D. F. G., Comisso, L., Peretti, E., Petropoulou, M., & Sironi, L. 2024, *ApJ*, 974, 75, doi: [10.3847/1538-4357/ad7021](https://doi.org/10.3847/1538-4357/ad7021)
- Frank, J., King, A., & Raine, D. 1992, *Accretion power in astrophysics.*, Vol. 21
- Ghisellini, G., Maraschi, L., & Tavecchio, F. 2009, *MNRAS*, 396, L105, doi: [10.1111/j.1745-3933.2009.00673.x](https://doi.org/10.1111/j.1745-3933.2009.00673.x)
- Ghisellini, G., Padovani, P., Celotti, A., & Maraschi, L. 1993, *ApJ*, 407, 65, doi: [10.1086/172493](https://doi.org/10.1086/172493)
- Ghisellini, G., Tavecchio, F., Foschini, L., et al. 2010, *MNRAS*, 402, 497, doi: [10.1111/j.1365-2966.2009.15898.x](https://doi.org/10.1111/j.1365-2966.2009.15898.x)
- Ghisellini, G., Tavecchio, F., Maraschi, L., Celotti, A., & Sbarrato, T. 2014, *Nature*, 515, 376, doi: [10.1038/nature13856](https://doi.org/10.1038/nature13856)
- Giommi, P., Padovani, P., & Polenta, G. 2013, *MNRAS*, 431, 1914, doi: [10.1093/mnras/stt305](https://doi.org/10.1093/mnras/stt305)
- Giommi, P., Padovani, P., Polenta, G., et al. 2012, *MNRAS*, 420, 2899, doi: [10.1111/j.1365-2966.2011.20044.x](https://doi.org/10.1111/j.1365-2966.2011.20044.x)
- H. E. S. S. Collaboration, Abramowski, A., Acero, F., et al. 2010, *A&A*, 516, A56, doi: [10.1051/0004-6361/201014321](https://doi.org/10.1051/0004-6361/201014321)
- . 2012, *A&A*, 538, A103, doi: [10.1051/0004-6361/201118406](https://doi.org/10.1051/0004-6361/201118406)
- Halpern, J. P., Chen, V. S., Madejski, G. M., & Chanan, G. A. 1991, *AJ*, 101, 818, doi: [10.1086/115725](https://doi.org/10.1086/115725)
- Hillas, A. M. 1984, *ARA&A*, 22, 425, doi: [10.1146/annurev.aa.22.090184.002233](https://doi.org/10.1146/annurev.aa.22.090184.002233)
- Hoshino, M. 2013, *ApJ*, 773, 118, doi: [10.1088/0004-637X/773/2/118](https://doi.org/10.1088/0004-637X/773/2/118)
- IceCube Collaboration, Aartsen, M. G., Ackermann, M., et al. 2018, *Science*, 361, eaat1378, doi: [10.1126/science.aat1378](https://doi.org/10.1126/science.aat1378)

- IceCube Collaboration, Abbasi, R., Ackermann, M., et al. 2022, *Science*, 378, 538, doi: [10.1126/science.abg3395](https://doi.org/10.1126/science.abg3395)
- Ichimaru, S. 1977, *ApJ*, 214, 840, doi: [10.1086/155314](https://doi.org/10.1086/155314)
- Inoue, Y., Khangulyan, D., & Doi, A. 2020, *ApJL*, 891, L33, doi: [10.3847/2041-8213/ab7661](https://doi.org/10.3847/2041-8213/ab7661)
- Inoue, Y., Khangulyan, D., Inoue, S., & Doi, A. 2019, *ApJ*, 880, 40, doi: [10.3847/1538-4357/ab2715](https://doi.org/10.3847/1538-4357/ab2715)
- Kafexhiu, E., Aharonian, F., Taylor, A. M., & Vila, G. S. 2014, *PhRvD*, 90, 123014, doi: [10.1103/PhysRevD.90.123014](https://doi.org/10.1103/PhysRevD.90.123014)
- Keivani, A., Murase, K., Petropoulou, M., et al. 2018, *ApJ*, 864, 84, doi: [10.3847/1538-4357/aad59a](https://doi.org/10.3847/1538-4357/aad59a)
- Kelner, S. R., & Aharonian, F. A. 2008, *PhRvD*, 78, 034013, doi: [10.1103/PhysRevD.78.034013](https://doi.org/10.1103/PhysRevD.78.034013)
- Khatee Zathul, A., Moulai, M., Fang, K., & Halzen, F. 2025, *ApJ*, 984, 54, doi: [10.3847/1538-4357/adc44d](https://doi.org/10.3847/1538-4357/adc44d)
- Kimura, S. S., Kashiyama, K., & Hotokezaka, K. 2021a, *ApJL*, 922, L15, doi: [10.3847/2041-8213/ac35dc](https://doi.org/10.3847/2041-8213/ac35dc)
- Kimura, S. S., Murase, K., & Mészáros, P. 2019, *PhRvD*, 100, 083014, doi: [10.1103/PhysRevD.100.083014](https://doi.org/10.1103/PhysRevD.100.083014)
- . 2021b, *Nature Communications*, 12, 5615, doi: [10.1038/s41467-021-25111-7](https://doi.org/10.1038/s41467-021-25111-7)
- Kimura, S. S., Murase, K., & Toma, K. 2015, *ApJ*, 806, 159, doi: [10.1088/0004-637X/806/2/159](https://doi.org/10.1088/0004-637X/806/2/159)
- Liodakis, I., Marscher, A. P., Agudo, I., et al. 2022, *Nature*, 611, 677, doi: [10.1038/s41586-022-05338-0](https://doi.org/10.1038/s41586-022-05338-0)
- Liu, J.-R., Wang, J.-M., Fermi-LAT Collaboration, et al. 2025, *Nature Astronomy*, doi: [10.1038/s41550-025-02538-2](https://doi.org/10.1038/s41550-025-02538-2)
- MAGIC Collaboration, Abe, K., Abe, S., et al. 2025, *A&A*, 695, A217, doi: [10.1051/0004-6361/202452785](https://doi.org/10.1051/0004-6361/202452785)
- Mahadevan, R. 1997, *ApJ*, 477, 585, doi: [10.1086/303727](https://doi.org/10.1086/303727)
- Maraschi, L., Ghisellini, G., & Celotti, A. 1992, *ApJL*, 397, L5, doi: [10.1086/186531](https://doi.org/10.1086/186531)
- Matthews, J. H., Bell, A. R., & Blundell, K. M. 2020, *NewAR*, 89, 101543, doi: [10.1016/j.newar.2020.101543](https://doi.org/10.1016/j.newar.2020.101543)
- Mbarek, R., Philippov, A., Chernoglazov, A., Levinson, A., & Mushotzky, R. 2024, *PhRvD*, 109, L101306, doi: [10.1103/PhysRevD.109.L101306](https://doi.org/10.1103/PhysRevD.109.L101306)
- Mingo, B., Hardcastle, M. J., Croston, J. H., et al. 2014, *MNRAS*, 440, 269, doi: [10.1093/mnras/stu263](https://doi.org/10.1093/mnras/stu263)
- Murase, K. 2022, *ApJL*, 941, L17, doi: [10.3847/2041-8213/aca53c](https://doi.org/10.3847/2041-8213/aca53c)
- Murase, K., Karwin, C. M., Kimura, S. S., Ajello, M., & Buson, S. 2024, *ApJL*, 961, L34, doi: [10.3847/2041-8213/ad19c5](https://doi.org/10.3847/2041-8213/ad19c5)
- Narayan, R., Mahadevan, R., & Quataert, E. 1998, in *Theory of Black Hole Accretion Disks*, ed. M. A. Abramowicz, G. Björnsson, & J. E. Pringle, 148–182, doi: [10.48550/arXiv.astro-ph/9803141](https://doi.org/10.48550/arXiv.astro-ph/9803141)
- Narayan, R., & Yi, I. 1994, *ApJL*, 428, L13, doi: [10.1086/187381](https://doi.org/10.1086/187381)
- Nemmen, R. S., Storchi-Bergmann, T., & Eracleous, M. 2014, *MNRAS*, 438, 2804, doi: [10.1093/mnras/stt2388](https://doi.org/10.1093/mnras/stt2388)
- Paliya, V. S., Domínguez, A., Ajello, M., Olmo-García, A., & Hartmann, D. 2021, *ApJS*, 253, 46, doi: [10.3847/1538-4365/abe135](https://doi.org/10.3847/1538-4365/abe135)
- Pei, Z., Fan, J., Yang, J., Huang, D., & Li, Z. 2022, *ApJ*, 925, 97, doi: [10.3847/1538-4357/ac3aeb](https://doi.org/10.3847/1538-4357/ac3aeb)
- Rees, M. J., Begelman, M. C., Blandford, R. D., & Phinney, E. S. 1982, *Nature*, 295, 17, doi: [10.1038/295017a0](https://doi.org/10.1038/295017a0)
- Rieger, F. M., Bosch-Ramon, V., & Duffy, P. 2007, *Ap&SS*, 309, 119, doi: [10.1007/s10509-007-9466-z](https://doi.org/10.1007/s10509-007-9466-z)
- Rieger, F. M., & Levinson, A. 2018, *Galaxies*, 6, 116, doi: [10.3390/galaxies6040116](https://doi.org/10.3390/galaxies6040116)
- Romero, G. E., & Vila, G. S. 2008, *A&A*, 485, 623, doi: [10.1051/0004-6361:200809563](https://doi.org/10.1051/0004-6361:200809563)
- Sahu, S., & Miranda, L. S. 2015, *European Physical Journal C*, 75, 273, doi: [10.1140/epjc/s10052-015-3519-1](https://doi.org/10.1140/epjc/s10052-015-3519-1)
- Sano, T., Inutsuka, S.-i., Turner, N. J., & Stone, J. M. 2004, *ApJ*, 605, 321, doi: [10.1086/382184](https://doi.org/10.1086/382184)
- Stawarz, Ł., & Petrosian, V. 2008, *ApJ*, 681, 1725, doi: [10.1086/588813](https://doi.org/10.1086/588813)
- Stecker, F. W. 1968, *PhRvL*, 21, 1016, doi: [10.1103/PhysRevLett.21.1016](https://doi.org/10.1103/PhysRevLett.21.1016)
- Stecker, F. W., Done, C., Salamon, M. H., & Sommers, P. 1991, *PhRvL*, 66, 2697, doi: [10.1103/PhysRevLett.66.2697](https://doi.org/10.1103/PhysRevLett.66.2697)
- Stickel, M., Padovani, P., Urry, C. M., Fried, J. W., & Kuehr, H. 1991, *ApJ*, 374, 431, doi: [10.1086/170133](https://doi.org/10.1086/170133)
- Sun, X., & Bai, X.-N. 2021, *MNRAS*, 506, 1128, doi: [10.1093/mnras/stab1643](https://doi.org/10.1093/mnras/stab1643)
- Tavecchio, F., Ghisellini, G., Ghirlanda, G., Foschini, L., & Maraschi, L. 2010, *MNRAS*, 401, 1570, doi: [10.1111/j.1365-2966.2009.15784.x](https://doi.org/10.1111/j.1365-2966.2009.15784.x)
- Toma, K., & Takahara, F. 2012, *ApJ*, 754, 148, doi: [10.1088/0004-637X/754/2/148](https://doi.org/10.1088/0004-637X/754/2/148)
- Urry, C. M., & Padovani, P. 1995, *PASP*, 107, 803, doi: [10.1086/133630](https://doi.org/10.1086/133630)
- Wakely, S. P., & Horan, D. 2008, in *International Cosmic Ray Conference*, Vol. 3, *International Cosmic Ray Conference*, 1341–1344
- Wang, J.-M., Staubert, R., & Ho, L. C. 2002, *ApJ*, 579, 554, doi: [10.1086/342875](https://doi.org/10.1086/342875)
- Wang, Z.-R., Liu, R.-Y., Petropoulou, M., et al. 2022, *PhRvD*, 105, 023005, doi: [10.1103/PhysRevD.105.023005](https://doi.org/10.1103/PhysRevD.105.023005)
- Woo, J.-H., & Urry, C. M. 2002, *ApJ*, 579, 530, doi: [10.1086/342878](https://doi.org/10.1086/342878)
- Woo, J.-H., Urry, C. M., van der Marel, R. P., Lira, P., & Maza, J. 2005, *ApJ*, 631, 762, doi: [10.1086/432681](https://doi.org/10.1086/432681)
- Xue, R., Huang, S.-T., Xiao, H.-B., & Wang, Z.-R. 2023, *PhRvD*, 107, 103019, doi: [10.1103/PhysRevD.107.103019](https://doi.org/10.1103/PhysRevD.107.103019)
- Xue, R., Liu, R.-Y., Petropoulou, M., et al. 2019, *ApJ*, 886, 23, doi: [10.3847/1538-4357/ab4b44](https://doi.org/10.3847/1538-4357/ab4b44)

- Xue, R., Liu, R.-Y., Wang, Z.-R., Ding, N., & Wang, X.-Y. 2021, *ApJ*, 906, 51, doi: [10.3847/1538-4357/abc886](https://doi.org/10.3847/1538-4357/abc886)
- Xue, R., & Wang, Z.-R. 2021, *Research in Astronomy and Astrophysics*, 21, 103, doi: [10.1088/1674-4527/21/4/103](https://doi.org/10.1088/1674-4527/21/4/103)
- Yan, D., Zeng, H., & Zhang, L. 2014, *MNRAS*, 439, 2933, doi: [10.1093/mnras/stu146](https://doi.org/10.1093/mnras/stu146)
- Yang, Q.-R., Liu, R.-Y., & Wang, X.-Y. 2025, *ApJ*, 980, 255, doi: [10.3847/1538-4357/adaea4](https://doi.org/10.3847/1538-4357/adaea4)
- Yuan, F. 2007, in *Astronomical Society of the Pacific Conference Series*, Vol. 373, *The Central Engine of Active Galactic Nuclei*, ed. L. C. Ho & J. W. Wang, 95, doi: [10.48550/arXiv.astro-ph/0701638](https://doi.org/10.48550/arXiv.astro-ph/0701638)
- Yuan, F., Cui, W., & Narayan, R. 2005, *ApJ*, 620, 905, doi: [10.1086/427206](https://doi.org/10.1086/427206)
- Yuan, F., & Narayan, R. 2014, *ARA&A*, 52, 529, doi: [10.1146/annurev-astro-082812-141003](https://doi.org/10.1146/annurev-astro-082812-141003)
- Yuan, F., Peng, Q., Lu, J.-f., & Wang, J. 2000, *ApJ*, 537, 236, doi: [10.1086/309020](https://doi.org/10.1086/309020)
- Yuan, F., Quataert, E., & Narayan, R. 2003, *ApJ*, 598, 301, doi: [10.1086/378716](https://doi.org/10.1086/378716)
- Yuan, F., Zdziarski, A. A., Xue, Y., & Wu, X.-B. 2007, *ApJ*, 659, 541, doi: [10.1086/512078](https://doi.org/10.1086/512078)
- Zhang, J., Liang, E.-W., Zhang, S.-N., & Bai, J. M. 2012, *ApJ*, 752, 157, doi: [10.1088/0004-637X/752/2/157](https://doi.org/10.1088/0004-637X/752/2/157)
- Zhang, J., Sun, X.-N., Liang, E.-W., et al. 2014, *ApJ*, 788, 104, doi: [10.1088/0004-637X/788/2/104](https://doi.org/10.1088/0004-637X/788/2/104)
- Zhao, X. Z., Yang, H. Y., Zheng, Y. G., & Kang, S. J. 2024, *ApJ*, 967, 104, doi: [10.3847/1538-4357/ad3ba9](https://doi.org/10.3847/1538-4357/ad3ba9)

Table 1. SED Fitting Parameters

Parameter	Symbol	1ES 0229+200	H2356–309	1ES 1101–232	1ES 0347–121	1ES 0414+009
Redshift	z	0.139	0.165	0.186	0.188	0.287
Leptonic Jet Model						
Electron Density Parameter	$N_{e,0}$ [cm^{-3}]	7×10^1	6×10^2	2.5×10^1	9×10^3	90
Spectral Index below Break	p_1	1.85	2.15	1.8	2.4	2.15
Spectral Index above Break	p_2	3.16	3.3	3.4	3	3.55
Minimum Lorentz Factor for Electrons	$\gamma_{e,\text{min}}$	1	2	5	1×10^2	90
Break Lorentz Factor for Electrons	$\gamma_{e,b}$	7×10^5	1.4×10^5	7.3×10^4	2×10^5	7.6×10^4
Maximum Lorentz Factor for Electrons	$\gamma_{e,\text{max}}$	7×10^6	1.4×10^6	7.3×10^5	2×10^6	1.5×10^5
*Variability Timescale	Δt [hr]	24	24	12	12	62.5
Doppler Factor	δ_D	8	20	20	20	30
Magnetic Field Strength	B_{jet} [G]	0.55	0.04	0.25	0.2	0.025
Lepto-hadronic ADAF Model						
* Mass of SMBH	M_{BH} [M_{\odot}]	1.75×10^9	3.98×10^8	1.02×10^9	4.47×10^8	2×10^9
* Accretion Rate	\dot{m}	4.25×10^{-4}	3×10^{-3}	2.7×10^{-3}	6.42×10^{-3}	7.3×10^{-3}
* Power-law Index for Radial Variation	s	0.3	0.3	0.3	0.3	0.3
* Shakura-Sunyaev Viscosity Parameter	α	0.3	0.3	0.3	0.3	0.3
* Ratio between the Gas and the Total Pressure	β	0.9	0.9	0.9	0.9	0.9
* Adiabatic Index	γ_{adi}	1.5	1.5	1.5	1.5	1.5
* Outer Radius of the ADAF	R_o [R_S]	10^4	10^4	10^4	10^4	10^4
Fraction of Energy to Electrons	δ_{ADAF}	0.1	0.5	0.4	0.5	0.5
Differential Proton Density at 1 eV	$N_{p,0}$ [$\text{cm}^{-3} \text{eV}^{-1}$]	2.5×10^{13}	2.5×10^{11}	1.6×10^{12}	1.5×10^{11}	3×10^{11}
Integrated Proton Density	N_p [cm^{-3}]	1.1×10^7	1.7×10^6	6.4×10^4	1.1×10^5	1.9×10^4
Proton Spectral Index	p	1.6	1.6	1.7	1.6	1.7
Proton Cutoff Energy	$\epsilon_{p,\text{cut}}$ [eV]	9×10^{13}	3×10^{13}	6×10^{13}	4×10^{13}	3×10^{13}
* Average Magnetic Field of ADAF	B_{ADAF} [G]	1	1	1	1	1
the pp Process						
Cold Proton Number Density	n_p [cm^{-3}]	1×10^{-4}	1.5	0.4	3	0.5

Notes. The values of M_{BH} for 1ES 0229+200, H2356–309, and 1ES 0347–121 are taken from [Woo & Urry \(2002\)](#), while those for 1ES 0414+009 and 1ES 1101–232 are adopted from [Falomo et al. \(2003\)](#) and [Paliya et al. \(2021\)](#), respectively.

* It indicates that the parameter values are fixed.

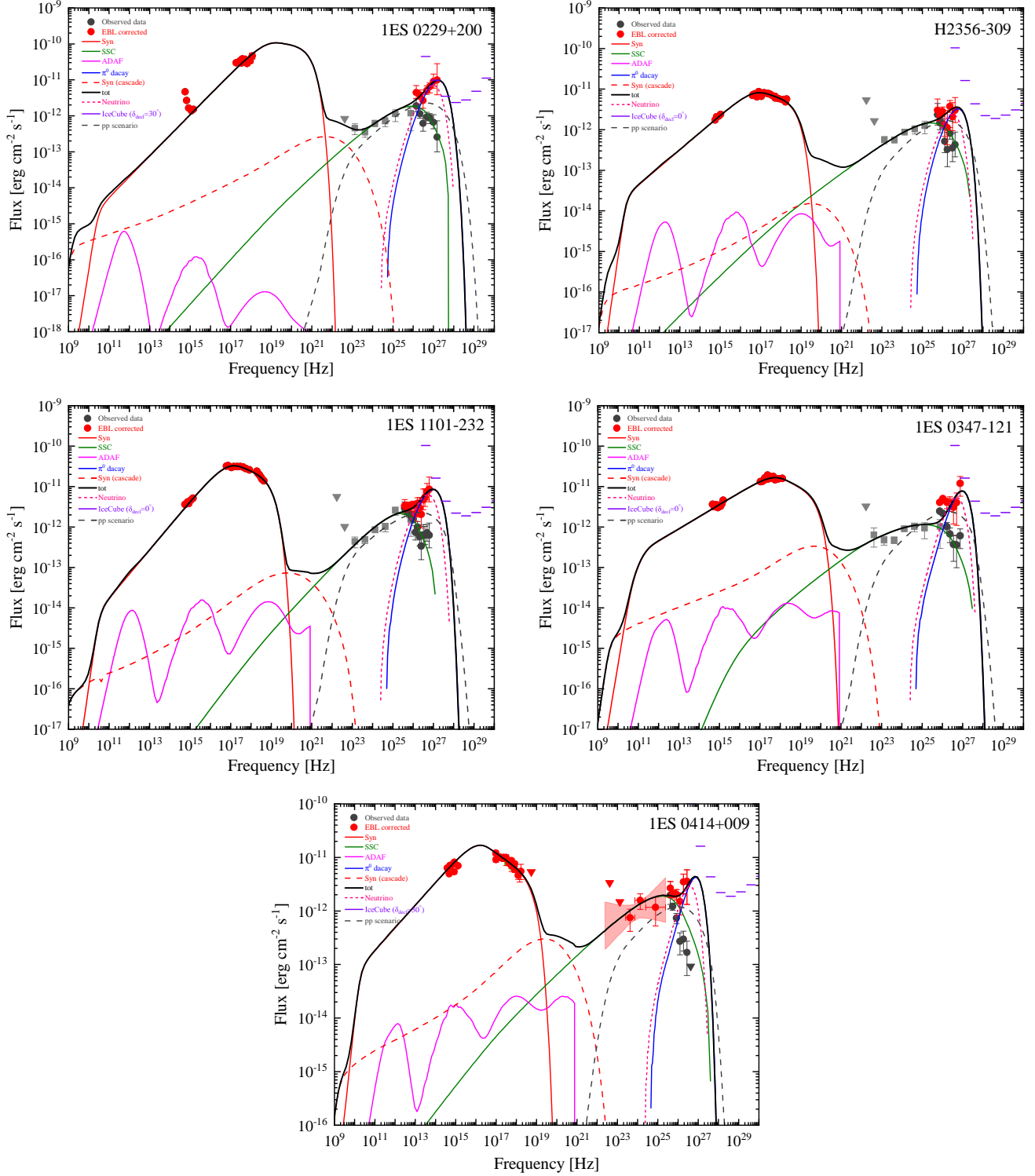


Figure 1. Broadband SEDs of the five BL Lacs with fitting results. The observational data, represented by scattered points, are referenced to Section 2. Gray circles and triangles denote data in the observer frame, whereas the corresponding red symbols indicate data corrected using the EBL model of [Finke et al. \(2022\)](#). The black solid lines represent the sum of each component emission for the sources, including the jet synchrotron radiation (red solid lines), the jet SSC radiation without EBL absorption (green solid lines), the ADAF spectrum (magenta solid lines), the γ -ray emission from the π^0 decay in the $p\gamma$ process (blue solid lines) and in the pp process (gray dashed lines), and the radiation from cascaded electrons (red and green dashed lines) produced by photomeson and Bethe–Heitler processes in the ADAF. The differential sensitivity curves (violet short horizontal lines) of IceCube are taken from [Aartsen et al. \(2019\)](#).

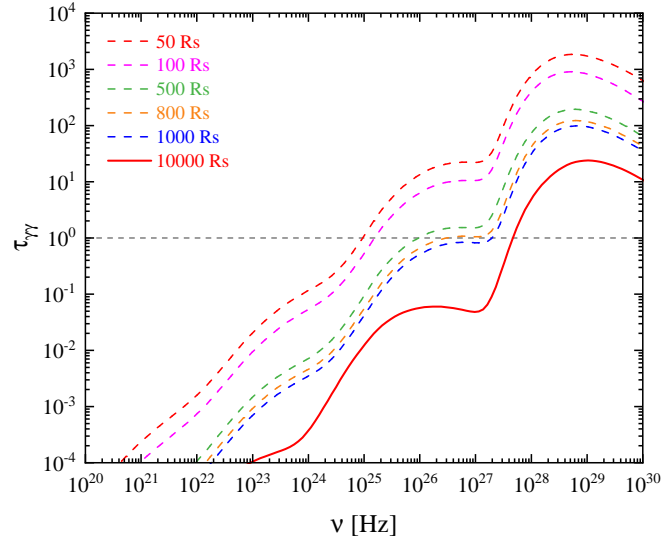


Figure 2. The $\gamma\gamma$ optical depth curves for the ADAF model with varying radii in the source 1ES 0347–121.